Optimal Design of Terminal Sliding Mode Controller for Direct Torque Control of SRMs

Xiaodong Sun, *Senior Member*, *IEEE*, Liyun Feng, *Student Member*, *IEEE*, Zhen Zhu, Gang Lei, *Member*, *IEEE*, Kaiai Diao, *Student Member*, *IEEE*, Youguang Guo, *Senior Member*, *IEEE*, and Jianguo Zhu, *Senior Member*, *IEEE*

***Abstract*- A nonsingular terminal sliding mode controller (NTSMC) based on a direct torque control is presented for a switched reluctance motor (SRM) in this paper. To guarantee dynamic stability, the nonsingular terminal sliding mode based on an improved reaching law is employed to design the speed controller. The torque ripple of the system can be suppressed, and the disturbance caused by uncertainties like load disturbance and parameter perturbation can be suppressed by the proposed NTSMC. Moreover, the gray wolf optimization algorithm is applied to automatically adjust the parameters of the controllers and the value of given flux, thereby acquiring a satisfactory result. The NTSMC is validated by both simulation and experimental results with a six-phase 12/10 SRM. Compared with PI and conventional sliding mode control, NTSMC improves the convergence rate of state and exhibits better performance in torque ripple reduction and anti-disturbance ability. The robustness and dynamic performance of the system can be ensured.**

Keywords: Direct torque control, switched reluctance motor, terminal sliding mode control, optimization algorithm

I. INTRODUCTION

Switched reluctance motors (SRMs) offer a competitive alternative in electric vehicles and hybrid electric vehicles [1], [2]. Compared with other several electrical machines, such as hybrid excited motors, permanent magnet motors [3], induction motors [4], SRMs without any windings and permanent magnets in the rotor have prominent advantages including low cost, wide range of speed, simple structure, and high reliability [5], [6].

The major obstacles for SRMs applications are the noise, vibration, and torque ripple [7], [8]. During the past decades, not only novel structures have been considered, but also a variety of control strategies have been investigated. Compared with the current chopping control and angle position control (APC) in the previous work, torque sharing function (TSF), direct instantaneous torque control (DITC), and direct torque control (DTC) are chosen as alternative strategies in the SRM drive system. A novel DITC was proposed to achieve wide operating range without an extra optimization strategy of the switching angle [9]. By contrast, the TSF optimization and the reference current calculation are not required. Based on a novel bus current sensor layout strategy under the soft-chopping mode, a DITC technique was studied in [10]. There are many unavoidable factors of conventional DTC due to inconstant switch frequency and torque ripple. Thus, the establishment of a novel voltage vector selection rule, increasing the number of levels in the power topology, and the introduction of pulse width modulation are effective ways to handle these problems [11-13].

In the control applications, the system is prone to be disturbed by the environment on the actual control aspect, resulting in the reduction of control accuracy. Therefore, sliding mode control (SMC) [14], model predictive control [15], adaptive control [16], robust control [17] and other control [18] technologies are employed to reduce the impact of interference. Among them, due to insensitivity to disturbance and parameter changes, SMC behaves better in robustness and anti-disturbance compared with the PI control. As an alternative, several advanced SMC has been investigated, such as adaptive SMC [19] with an integral sliding mode surface independent of the number of fuzzy rules, second-order sliding-mode [20], terminal SMC (TSMC), SMC with advanced reaching laws [21]. Among them, TSMC itself has robustness and anti-disturbance capability, which can converge in finite time. In addition, advanced reaching law such as the super-twisting algorithm can be employed in TSMC or other types of SMCs to improve the performance [22], [23].

As for TSMC, an equivalent-control-based fast TSMC law was designed in [24] by constructing a novel terminal sliding surface to solve the position tracking control problem for the permanent magnet linear motor. In [25], a novel nonsingular TSMC (NTSMC) with fast convergence speed and good tracking accuracy is designed. By compositing the NTSMC, a high-accuracy control strategy was presented to minimize the estimation error [26]. As reported in [27], a practical TSMC framework based on an adaptive disturbance observer was

Manuscript received Feb. 19, 2021; revised May 16, 2021 and Jul. 21, 2021; accepted Sep. 07, 2021. This work was supported by the National Natural Science Foundation of China under Project 51875261, the Natural Science Foundation of Jiangsu Province of China under Project BK20180046, the Postgraduate Research & Practice Innovation Program of Jiangsu Province under Project KYCX21_3332, and the State Scholarship Fund of China Scholarship Council under Grant 202108320319. *(Corresponding author: Zhen Zhu)*

X. Sun, L. Feng, Z. Zhu and K. Diao are with the Automotive Engineering Research Institute, Jiangsu University, Zhenjiang 212013, China (email: xdsun@ujs.edu.cn, fly_95@163.com, zhuzhenjs@126.com, diaokaikai@163.com).

G. Lei and Y. Guo are with School of Electrical and Information Engineering, University of Technology Sydney, NSW 2007, Australia, (e-mail: gang.lei@uts.edu.au, Youguang.Guo1@uts.edu.au).

J. Zhu is with the School of Electrical and Information Engineering, University of Sydney, NSW, 2006, Australia (e-mail: jianguo.zhu@sydney.edu.au).

applied in suspension systems. However, the application of the TSMC to the SRM is relatively rare.

However, complex control parameters also raise some difficulty, which influences the performance. Recently, some optimization algorithms, such as genetic algorithm [28], particle swarm optimization [29], the grey wolf optimization algorithm (GWOA) [30] and the coyote optimization algorithm (COA) [31] have been employed to optimize the tuned parameters. Among them, the GWOA presents superiority in local search capability, solution accuracy, and convergence. Moreover, the GWOA has better operability and fast operation speed based on parallel computing of objective function.

In this paper, TSMC applied in the speed controller and GWOA automatically tuning the parameters are combined to improve the dynamic performance and robustness. The anti-disturbance capability is enhanced for the uncertainties caused by load disturbance and parameter perturbation without increasing the difficulty of modeling the control system. Section II presents the DTC system based on speed controller using the proposed NTSMC considering uncertain factors. An improved adaptive reaching law is introduced to suppress uncertainties and ensure fast convergence. In Section III, the GWOA is discussed in detail and applied to design tuning parameters of the controller and the value of given flux in the DTC system. Simulation and experimental validations of the control method with PI, SMC, and NTSMC respectively are given in Sections IV and V, followed by the conclusion in Section VI.

II. DITC System Based on Speed Controller

A. Structure and Mathematic Model of SRM

Fig. 1 shows the structure of the studied 12/10 six-phase SRM [32], in which the excited poles of the stator are wound by six-phase windings. The mechanical motion equation of the SRM is

$$T_e^* - T_L - D \cdot \omega - J\frac{d\omega}{dt} = 0 \tag{1}$$

where T_e^* is the given reference torque, T_L is the load torque, ω represents the angular speed, D and J represent the coefficient of friction and the rotational inertia, respectively.

Considering the internal parameter perturbation and the external disturbances, (1) is given as

$$\frac{d\omega}{dt} = \frac{1}{J}\left(T_e^* - D \cdot \omega\right) + r \tag{2}$$

where r represents the sum of disturbances.

In (2), r can be specifically expressed as

$$r = \Delta a \cdot \omega + \Delta b \cdot T_e^* + \Delta T_L \tag{3}$$

where Δa and Δb represent uncertain factors caused by parameter variations, and ΔT_L is load disturbance.

Therefore, the state equation of torque is shown as

$$\dot{\omega} = -\frac{D}{J}\omega + \frac{1}{J}T_e^* + r \tag{4}$$

where $\dot{\omega} = d\omega / dt$.

B. Direct Torque Control Strategy

Fig. 2 shows the control block diagram of the DTC system, including the SRM model, power converter, speed controller, switch modular, interval judgment, and flux and torque calculation. The speed loop adopts the NTSMC based on the improved reaching law, and combines the GWOA to enhance the performance of the control system.

Fig. 1. A prototype of the SRM.

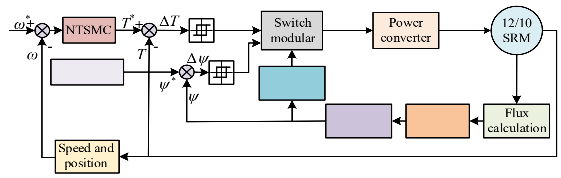

Fig. 2. Control block diagram of the DTC system.

C. An Improved Reaching Law

To further suppress the chattering and increase convergence speed correspondingly, an improved RL is designed as

$$\frac{ds}{dt} = -\frac{k_1}{\delta + (1-\delta)e^{-\alpha|s|}} sigmoid(s) - k_2 |s|^{\beta} s \tag{5}$$

where $sigmoid(s)=2/(1+e^{-cs})-1$, $c>0$, $k_1>0$, $k_2>0$, $0<\delta<1$, $\alpha>1$, $0<\beta<2$.

Compared with the conventional RL, the improved RL introduces the variable gain term and the power terminal of the system state variable. Obviously, the variable gain term $k_1/[\delta+(1-\delta)e^{-\alpha|s|}]$ converges to 1 when the system trajectory approaches the switching surface, which suppresses the chattering. The variable gain term converges to k_1/δ when the state point is far away from the switching surface, which is larger than k_1. Thus, the approaching speed of the system can be further improved. The $sign(s)$ function in the improved RL can be replaced by the $sigmoid(s)$ function with smooth continuous characteristics to consider the practical engineering application. Besides, the power term $|s|^{\beta}$ is added among the pure exponential approach term, and accelerates the convergence at the initial approaching stage.

To validate the stability of the improved RL, the Lyapunov function $V=s^2/2$ is selected. Then, the following equation can be obtained.

$$\dot{V} = s\dot{s} = -\frac{k_1 s}{\delta + (1-\delta)e^{-\alpha|s|}} sigmoid(s) - k_2 |s|^{\beta} s^2 \tag{6}$$

According to (6), due to $s \cdot sigmoid(s) \geqslant 0$, $k_1>0$, $k_2>0$, $0<\delta<1$, $\alpha>0$, $0<\beta<1$, $|s|>0$, it is obvious that Lyapunov stability condition (7) can be satisfied.

$$\dot{V} = s\dot{s} \leq 0 \tag{7}$$

As a result, RL designed in this paper can ensure that the trajectory of the system reaches the equilibrium point in a finite time.

D. Design of Speed Controller

Terminal sliding mode control is realized by constructing a nonlinear sliding mode surface equation, which achieves full tracing in the specified limited time under the premise of ensuring stability. As known, the boundary of the uncertainty range of the system is usually required to be known for conventional SMC, which is difficult to achieve in practical engineering [33-35]. Thus, adaptive SMC is preferred to solve the problem of uncertainty or time-varying parameter systems by combining SMC and adaptive control.

According to the above analysis, the adaptive nonsingular terminal sliding mode is introduced into the speed controller for the better anti-disturbance ability of the system.

The speed controller is to make the actual speed ω accurately track the reference speed ω^* in real-time and be robust to disturbance brought by uncertain factors. The speed error e can be defined as

$$e = \omega^* - \omega \tag{8}$$

Then, based on the basic steps of controller design, the integral sliding mode surface s is given by

$$s = e + \lambda \int e dt \tag{9}$$

where λ is the design constant.

Substituting (8) and (9) into (2), we have

$$T_{e1} = (J\lambda - D)e + D\omega^* \tag{10}$$

where T_{e1} is the torque without uncertain factors r, and the derivative of the reference speed ω^* is 0.

Since both the parameter perturbation and load disturbance are not taken into account, T_{e1} does not affect suppressing strong disturbance. Let the uncertainty control quantity $T_{e2}= T_e^*$ - T_{e1}, then the derivative of e can be expressed as

$$\dot{e} = -\frac{1}{J}(T_{e1} + T_{e2}) + \frac{D}{J}(\omega^* - e) - r . \tag{11}$$

Selecting the sliding-mode surface σ as

$$\sigma = e - \int_0^t \left(-\frac{1}{J} T_{e1} + \frac{D}{J}(\omega^* - e) \right) dt . \tag{12}$$

Combining (11) and (12), the following expression is obtained.

$$\dot{\sigma} = -\frac{1}{J} T_{e2} - r . \tag{13}$$

Next, it can be obtained that

$$\ddot{\sigma} = -\frac{1}{J} \dot{T}_{e2} - \dot{r} . \tag{14}$$

Furthermore, the following nonsingular terminal sliding mode surface z is written as

$$z = \sigma + \eta \dot{\sigma}^{p/q} \tag{15}$$

where η>0, 0<p/q<1, and p and q represent positive odd numbers, respectively.

Taking the time derivative of the nonsingular terminal sliding-mode surface yields

$$\dot{z} = \dot{\sigma} + \eta \frac{p}{q} \dot{\sigma}^{p/q-1} \ddot{\sigma} . \tag{16}$$

Simultaneously, substituting the improved RL (5) into (16) can get the following result.

$$\ddot{\sigma} = \frac{q}{\eta p} \dot{\sigma}^{1-p/q} \left(-\frac{k_1 \cdot sigmoid(z)}{\delta + (1-\delta)e^{-\alpha|z|}} - k_2 |z|^\beta z - \dot{\sigma} \right) \tag{17}$$

Combining (17) and (14), the uncertainty control quantity T_{e2} can be calculated as

$$T_{e2} = J \int_0^t \left(\frac{q}{\eta p} \dot{\sigma}^{1-p/q} \left(\frac{k_1 \cdot sigmoid(z)}{\delta + (1-\delta)e^{-\alpha|z|}} + k_2 |z|^\beta z + \dot{\sigma} \right) \right) dt \tag{18}$$

where the uncertain factors r is the slow time-varying with time, and the derivative of r is 0. As a result, combining (11) and (18), T_e eventually can be calculated.

The stability of the speed controller is analyzed below. Based on $V=s^2/2$, the condition of sliding mode arrival is satisfied when the following formula is established.

$$\dot{V} = z\dot{z} \le 0 \tag{19}$$

Combining (14) and (17), we have

$$\begin{aligned} \dot{V} &= z\left(\dot{\sigma} + \eta \frac{p}{q} \dot{\sigma}^{p/q-1} \left(-\frac{1}{J}\dot{T}_{e2} - \dot{r}\right) \right) \\ &= z\left(-\frac{k_1 \cdot sigmoid(z)}{\delta + (1-\delta)e^{-\alpha|z|}} - k_2 |z|^\beta z \right) \le 0 \end{aligned} \tag{20}$$

According to the above analysis, the stability of the control system is ensured, and the system chattering can be suppressed by reasonable control parameters. Fig. 3 illustrates the structure diagram of the NTSMC under uncertainties.

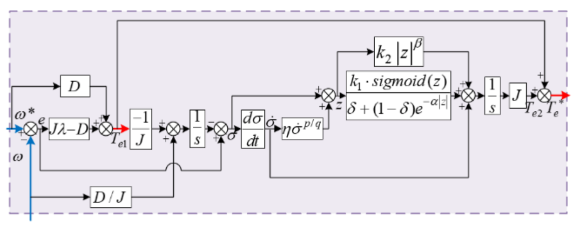

Fig. 3. Schematic diagram of NTSMC.

III. Application of GWOA for Autotuning

The proposal of GWOA was inspired by wolves' hunting, which mimics the strict hierarchy behavior [36-38]. The gray wolves are divided into the wolf α, β, δ, and θ based on their fitness values, from high to low. The encircling models of the gray wolf are shown as follows:

$$\vec{A} = 2 \cdot \vec{a} \cdot \vec{r}_1 - \vec{a} \tag{21}$$

$$\vec{C} = 2 \cdot \vec{r}_2 \tag{22}$$

$$\vec{D} = \left| \vec{C} \cdot \vec{X}_m - \vec{X} \right| \tag{23}$$

$$\vec{X}(t+1) = \left| \vec{X}_m - \vec{A} \cdot \vec{D} \right| \tag{24}$$

where the subscript m denotes α, β and δ, respectively, t is the current iteration number, $\vec{r}_1$ and $\vec{r}_2$ are random vectors in [0, 1], $\vec{a}$ is linearly decreased from 2 to 0 throughout iterations. $\vec{D}$ is the distance between the gray wolf and prey, $\vec{C}$ and $\vec{A}$

are coefficient vectors, $\vec{X}$ and $\vec{X}_m$ represent the position vector of the gray wolf and prey.

The hunting model of the gray wolf can be expressed as follows:

$$\vec{D}_m = \left|\vec{C}\cdot\vec{X}_m - \vec{X}\right| \tag{25}$$

$$\vec{X}_n = \vec{X}_m - \vec{A}\cdot\vec{D}_m \tag{26}$$

$$\vec{X}(t+1) = \frac{\vec{X}_1 + \vec{X}_2 + \vec{X}_3}{3} \tag{27}$$

where n denotes 1, 2 and 3, respectively, and $\vec{X}_n$ is the movement instructions given by α, β and γ, respectively. The GWOA has high convergence rate, strong local search capability and operability.

From selection experience on the models, the control parameters α, β, and δ have little influence on the performance, thus k_1, k_2, p, q, and η are chosen as the primary optimization parameters. Take the optimization parameters k_1 as an example, the upper bounds and lower bounds are selected as 1×10^{-3} and 1×10^{6} based on the stability condition to find the optimal solution within a large range of values at first. Then, we use the dichotomy method for parameter debugging to narrow the range of parameters to improve efficiency, which is a trial by experience. In addition, given flux linkage f is set as a tunable parameter for lower torque ripple. Therefore, before the optimization, the relevant values of the GWOA are selected in Table I.

TABLE I
PARAMETERS OF THE GWOA

Parameter	Value
Number of wolves, n	30
Coefficients, k_1, k_2	[10, 1000]
Coefficients, η,	[0,10]
Coefficients, p/q,	[0,1]
Parameters, g	[0.1, 0.2]

The fitness function should be defined to select the parameters automatically. Based on the major control objectives including minimum speed error and torque ripple, the objective function is designed as

$$F = \frac{1}{N}\sum_{n=0}^{N}[\left|\Delta e_{\omega}(n)\right| nTs + \left|\Delta e_t(n)\right| nTs] \tag{28}$$

where $\Delta e_{\omega}(n)$ and $\Delta e_t(n)$ are the sampling speed error and the sampling torque error, respectively.

The torque ripple of SRM is expressed as [12]

$$k = \frac{T_{\max} - T_{\min}}{T_{avg}} \times 100\% \tag{29}$$

where k is the torque ripple coefficient, $T_{\max}$ and $T_{\min}$ are the maximum torque and the minimum torque, and T_{avg} represents the average torque.

The evolution of the fitness value of GWOA is shown in Fig. 4. As shown, the value of F decreases rapidly in the iterations in the initial stage. The maximum number of iterations is 80, and the best fitness index after 40 iterations is F=4.2×10^{6}.

VI. SIMULATION RESULTS

To clearly show the strong robustness and anti-interference ability of the NTSMC, the results of the PI and SMC using conventional exponential RL are given for comparison. The block diagrams of the PI and SMC using the conventional exponential RL are presented in Fig. 5 and 6.

The inertia J is 7.9×10^{-4} kg.m^2 and D is 1×10^{-3} in the control system built in Matlab/Simulink. Due to the high switching frequency in the high-speed range and the principle of DTC, the reference speed of the SRM is set as 1000 rpm, which is more suitable for low and medium-speed operation. The turn-on and turn-off angles are -5°and 11°. As for the PI controller, the optimal proportional and integral parameters are 0.069 and 11.3. To ensure the comparability of results between SMC and NTSMC, the switching gain and linear gain both keep the same. The optimal parameters of SMC and NTSMC using GWOA are: k_1 = 130, k_2 = 20, δ = 0.5, α = 2, β = 0.3, p = 5, q = 7, η = 0.9. In addition, the given flux value g after optimization of three controllers is set as 0.15 Wb.

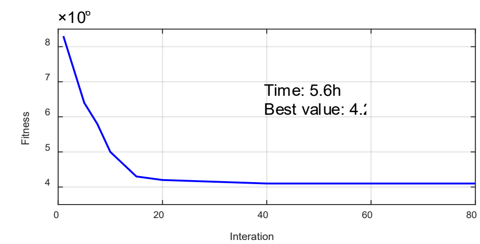

Fig. 4. Evolution of fitness value of GWOA.

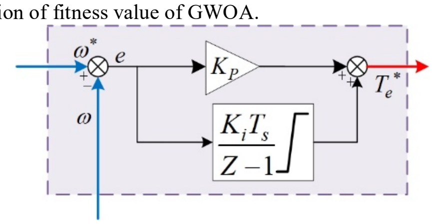

Fig. 5. Block diagram of PI control.

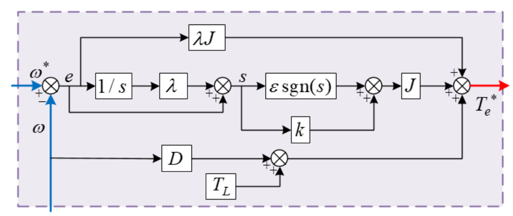

Fig. 6. Block diagram of SMC.

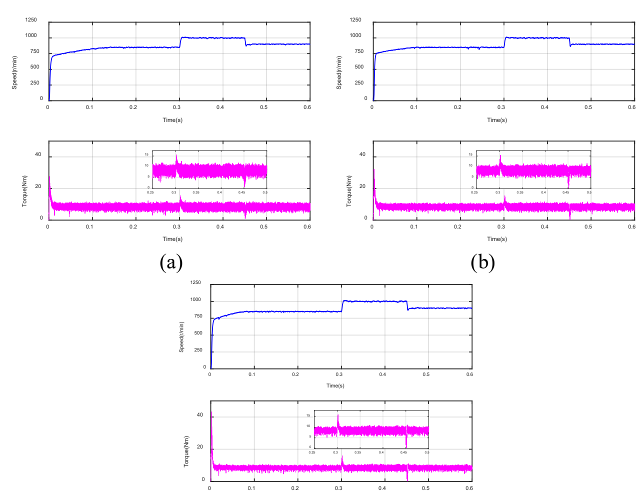

(a) (b)

(c)

Fig. 7. Speed and torque when the speed changes under 8 Nm, (a) PI, (b) SMC, and (c) NTSMC.

Fig. 7 shows the speed and torque curves when the speed changes from 850 to 1000 rpm at 0.3 s and from 1000 to 900 rpm at 0.45 s under 8 Nm. As shown, the startup time of using NTSMC is 0.08 s, which is smaller than those of using PI (0.13 s) and SMC (0.1 s). The dynamic response time has no significant difference between the three methods. It can be seen that the NTSMC exhibits the fastest acceleration and the lowest torque ripples.

Fig. 8 shows the speed and torque responses of PI, SMC, and NTSMC in the DTC control of an SRM under 8 Nm at 1000 rpm. As shown, the startup time of using NTSMC is 0.07 s, which is smaller than those of using PI (0.16 s) and SMC (0.11 s). Thus, the control system with NTSMC approaches the fastest. The maximum and minimum torque values of NTSMC are 10.8 and 6.25 Nm, respectively, while those of PI are 11.3 and 5.7 Nm, and those of SMC are 11 and 5.9 Nm, respectively. Thus, the torque ripples of PI, SMC, and NTSMC are 65.9 %, 60.3%, and 53.4%, respectively. NTSMC can reduce the torque ripple by 12.5% and 6.9%, respectively, compared with PI and SMC.

Fig. 9 shows the speed and torque responses of PI, SMC, and NTSMC when a step load torque (from 8 to 12 Nm) is applied at 0.3 s. As shown, all controllers can restore the SRM to the stable speed under the load disturbance. PI, SMC, and NTSMC take about 0.13, 0.11, and 0.09 s to return to the reference speed, respectively. Besides, the over-speed shootings under them are 135, 99, and 83 rpm, respectively. In the steady state, the maximum and minimum torque values are 15 and 11 Nm for the NTSMC, 15.8 and 10.1 Nm for the PI, and 15.2 and 10.4 Nm for the SMC. Therefore, the torque ripple of SRM under NTSMC has been reduced from 53.4% to 31%. This is better than the torque ripple reductions of PI (from 65.9% to 44%) and SMC (from 60.3% to 37.5%).

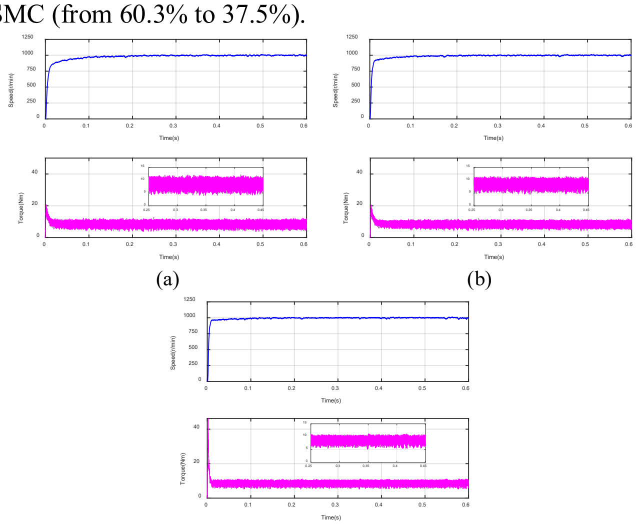

Fig. 8. Speed and torque under 8 Nm, (a) PI, (b) SMC, and (c) NTSMC.

Fig. 10 shows the simulation results when the parameter perturbations $\Delta a = 0.003$, $\Delta b T_e^* = 4$ N are applied at 0.3 s. As shown, the SRM with PI, SMC, and NTSMC methods spend about 0.14, 0.11, and 0.08 s to return to the reference speed, respectively. The speed overshooting is 63 rpm, which is decreased by 42.7% and 23.2%, respectively, compared with those with PI (110 rpm) and SMC (82 rpm). When the torque reaches the steady state, the maximum and minimum torque values of PI, SMC, and NTSMC are 7.3 and 1.4 Nm, 7.1 and 1.7 Nm, 6.8 and 2.2 Nm, respectively. The phase current waveforms under 8 Nm and 12 Nm are presented in Figs. 11 and 12. As shown, the current waveforms of different controllers under the same control strategy are similar. Besides, the amplitude of the current waveform under 12 Nm is larger than that under 8 Nm. Table II lists the main performance results of the simulation.

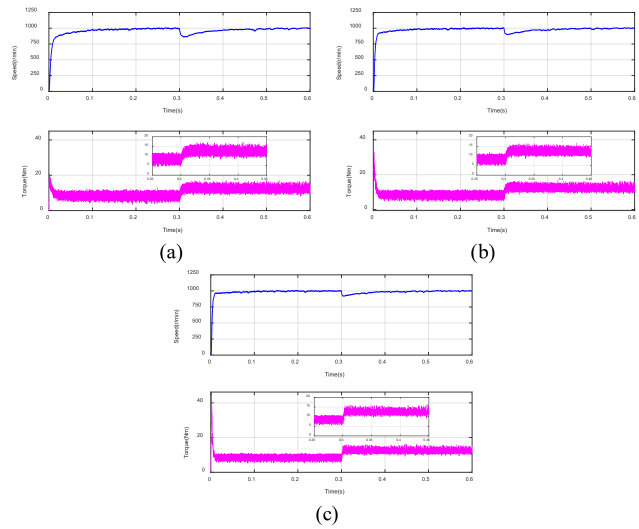

Fig. 9. Speed and torque when the load torque changes, (a) PI, (b) SMC, and (c) NTSMC.

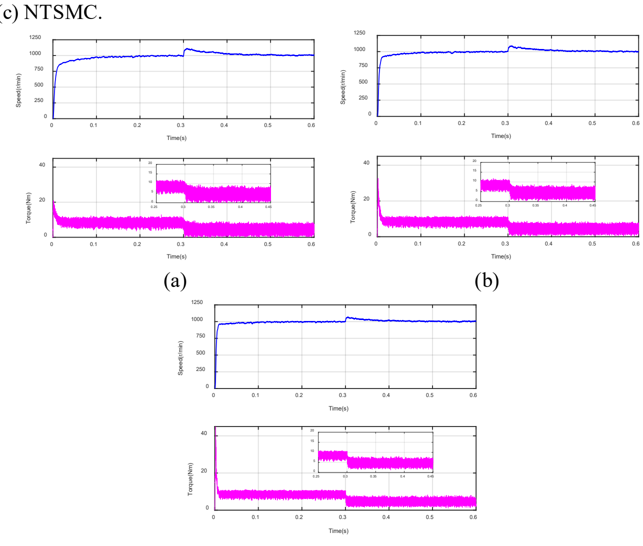

Fig. 10. Speed and torque when parameters change, (a) PI, (b) SMC, and (c) NTSMC.

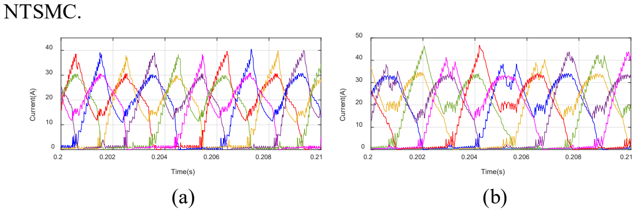

Fig. 11. Phase current using PI and SMC, (a) under 8 Nm, (b) under 12 Nm.

Although all three controllers can return to a steady state when the disturbance caused by load disturbance and parameter perturbation occurs, the NTSMC is more effective. NTSMC has the superiority of shorter speed response time, larger torque ripple reduction, and better anti-disturbance ability. Compared with the PI and traditional SMC, NTSMC has stronger robustness against uncertainties like the load torque disturbance and parameter perturbation.

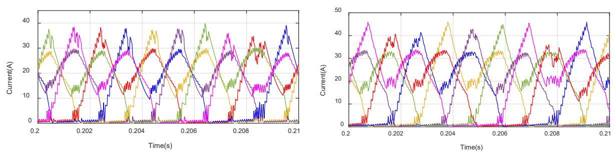

(a) (b)

Fig. 12. Phase current using NTSMC, (a) under 8 Nm, (b) under 12 Nm.

TABLE II
SIMULATION RESULTS

	PI	SMC	NTSMC
Speed startup time	0.16 s	0.11 s	0.07 s
Torque ripple	65.9%	60.3%	53.4%
Speed oscillation when the load torque changes	135 rpm	99 rpm	83 rpm
Speed oscillation when parameters change	110 rpm	82 rpm	63 rpm

As shown in Fig. 14, the speed and torque of three methods can perform well when speed changes. The speed startup time of PI, SMC and NTSMC are 0.15 s, 0.12 s and 0.1 s, respectively. Fig. 15 shows the experimental speed and torque results under 8 Nm at 1000 rpm. The rise-up time using NTSMC is about 0.11 s while those of PI and SMC are 0.2 s and 0.18 s, respectively. Thus, NTSMC has faster acceleration. Besides, the NTSMC behaves well in torque ripple reduction compared with that of PI and SMC. To be specific, the torque ripples under PI, SMC and NTSMC are 87.5 %, 71.2 %, and 60 %, respectively. The experimental results when the disturbances are caused by uncertainties are shown in Figs. 16 and 17, respectively. As shown, the over shootings of the speed waveform pulsation under PI, SMC and NTSMC are 169 rpm, 131 rpm, and 106 rpm, respectively, when the load torque changes (from 8 to 12 Nm). When parameters are perturbed, the speed overshooting under NTSMC is 67 rpm, which is decreased by 40.2% and 30.9%, respectively, compared with that of PI (112 rpm) and SMC (97 rpm). It can be seen that the anti-disturbance capability of NTSMC is more prominent when the same load disturbance and parameter perturbation apply. Fig. 18 shows the phase current waveforms under 8 Nm and 12 Nm. As shown, the peak current of NTSMC is slightly smaller than other two methods and the phase current waveform is similar. Besides, it is obviously found that the current amplitude is positively correlated with the load torque.

Table III tabulates the comparison of experimental results in terms of three control systems, which verifies the effectiveness of NTSMC. As shown in the experimental results in four operation conditions, the proposed NTSMC exhibits better performance in response speed, torque ripple reduction, robustness, and anti-disturbance ability. Moreover, the peak current and the current rate of change are also maintained without increasing the copper loss. In summary, the comprehensive performance of NTSMMC is superior to PI and SMC based on the simulation and experimental results.

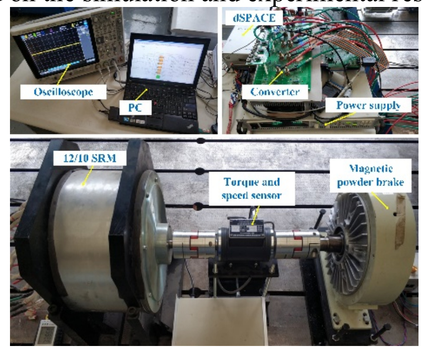

Fig. 13. The experimental test platform.

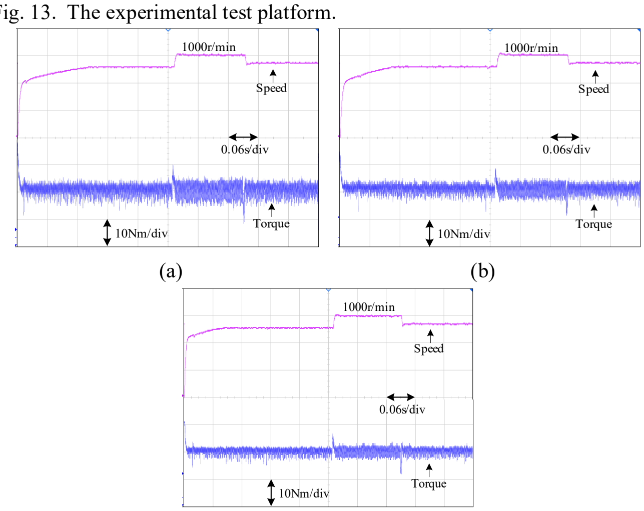

(a) (b) (c)

Fig. 14. Speed and torque when the speed changes under 8 Nm, (a) PI, (b) SMC, and (c) NTSMC.

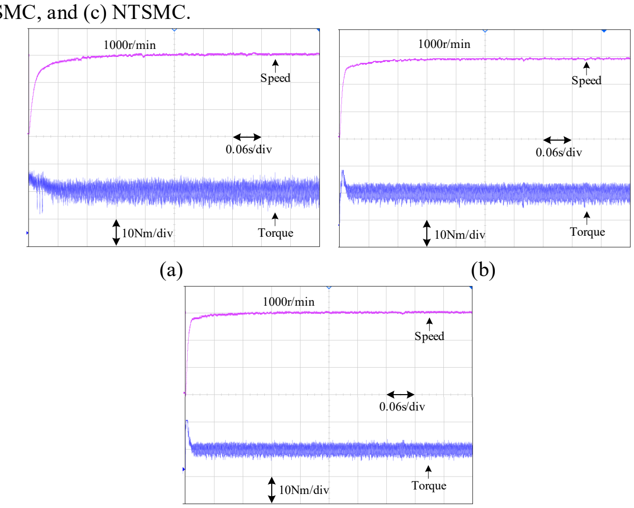

(a) (b) (c)

Fig. 15. Speed and torque under 8 Nm, (a) PI, (b) SMC, and (c) NTSMC.

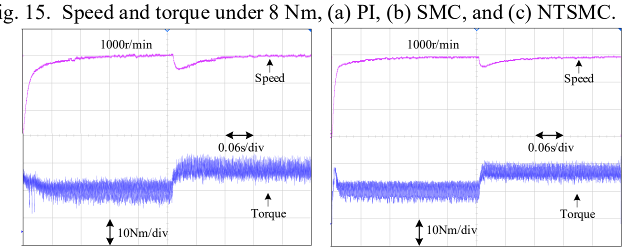

(a) (b)

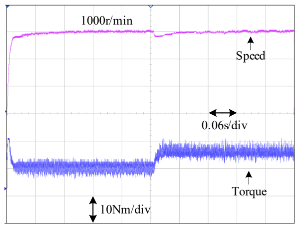

(c)

Fig. 16. Speed and torque when the load torque changes, (a) PI, (b) SMC, and (c) NTSMC.

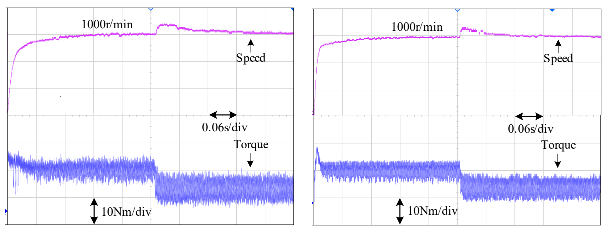

(a) (b)

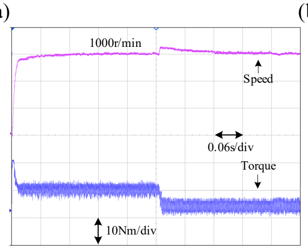

(c)

Fig. 17. Speed and torque when parameters change, (a) PI, (b) SMC, and (c) NTSMC.

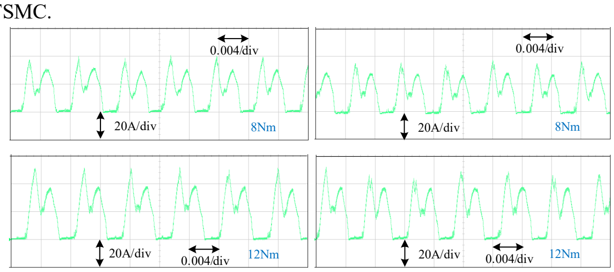

(a) (b)

Fig. 18. Phase current under 8 Nm and 12 Nm, (a) using PI and SMC, (b) using NTSMC.

TABLE III
EXPERIMENTAL RESULTS

	PI	SMC	NTSMC
Speed startup time	0.2 s	0.18 s	0.11 s
Torque ripple	87.5%	71.2%	60%
Speed oscillation when the load torque changes	169 rpm	131 rpm	106 rpm
Speed oscillation when parameters change	112 rpm	97 rpm	67 rpm

VI. CONCLUSION

This paper proposed an improved DTC system to effectively reduce torque ripples and enhance the robustness, response speed and anti-disturbance ability of an SRM drive system. In the study, the superiority of the NTSMC based on an improved RL on torque ripple reduction and the convergence rate of the state is obvious. Meanwhile, the disturbance caused by uncertainties like load disturbance and parameter perturbation was further suppressed. Moreover, the GWOA is introduced to automatically tune the parameters including speed controller and given flux for accurate tracking of speed and minimizing torque ripple. The combination of the NTSMC and GWOA improves the robustness and dynamic performance of the system. Compared with PI and SMC, the advantages of improved NTSMC applied in the DTC system have been verified by simulations and experiments with a 12/10 SRM.

REFERENCES

[1] X. Sun, Z. Shi, G. Lei, Y. Guo, and J. Zhu, “Analysis and design optimization of a permanent magnet synchronous motor for a campus patrol electric vehicle,” *IEEE Trans. Veh. Technol.,* vol. 68, no. 11, pp. 10535-10544, Nov. 2019.

[2] S. Kim and S. B. Choi, “Cooperative control of drive motor and clutch for gear shift of hybrid electric vehicles with dual-clutch transmission,” *IEEE/ASME Trans. Mechatron.*, vol. 25, no. 3, pp. 1578-1588, 2020.

[3] Z. Shi, et al, “Robust design optimization of a five-phase PM hub motor for fault-tolerant operation based on Taguchi method,” *IEEE Trans. Energy Convers.*, vol. 35, no. 4, pp. 2036-2044. Dec. 2020.

[4] M. J. Duran, I. Gonzalez-Prieto, N. Rios-Garcia, and F. Barrero, “A simple, fast, and robust open-phase fault detection technique for six-phase induction motor drives,” *IEEE Trans. Power Electron.*, vol. 33, no. 1, pp. 547-557, Jan. 2018.

[5] X. Sun, L. Feng, K. Diao, and Z. Yang, “An improved direct instantaneous torque control based on adaptive terminal sliding mode for a segmented-rotor SRM,” *IEEE Trans. Ind. Electron.*, vol. 68, no. 11, pp. 10569-10579, Nov. 2021.

[6] S. Song, G. Fang, R. Hei, J. Jiang, R. Ma, and W. Liu, “Torque ripple and efficiency online optimization of switched reluctance machine based on torque per ampere characteristics,” *IEEE Trans. Power Electron.*, vol. 35, no. 9, pp. 9608-9616, Sep. 2020.

[7] K. Diao, X. Sun, G. Lei, Y. Guo, and J. Zhu, “Multiobjective system level optimization method for switched reluctance motor drive systems using finite element model,” *IEEE Trans. Ind. Electron.*, vol. 67, no. 12, pp. 10055-10064, Dec. 2020.

[8] W. Wang, J. Zhao, Y. Zhou and F. Dong, "New optimization design method for a double secondary linear motor based on R-DNN modeling method and MCS optimization algorithm," *Chinese Journal of Electrical Engineering*, vol. 6, no. 3, pp. 98-105, Sept. 2020.

[9] H. Zeng, H. Chen, and J. Shi, “Direct instantaneous torque control with wide operating range for switched reluctance motors,” *IET Electric Power Applications*, vol. 9, no. 9, pp. 578-585, Nov. 2015.

[10] C. Gan, J. Wu, Q. Sun, S. Yang, Y. Hu, and L. Jin, “Low-cost direct instantaneous torque control for switched reluctance motors with bus current detection under soft-chopping mode,” *IET Power Electronics*, vol. 9, no. 3, pp. 482-490, Mar. 2016.

[11] X. Sun, K. Diao, Z. Yang, G. Lei, Y. Guo, and J. Zhu, “Direct torque control based on a fast modeling method for a segmented-rotor switched reluctance motor in HEV application,” *IEEE J. Emerg. Sel. Top. Power Electron.*, vol. 9, no. 1, pp. 232-241, Feb. 2021.

[12] N. Yan, X. Cao, and Z. Deng, “Direct torque control for switched reluctance motor to obtain high torque-ampere ratio,” *IEEE Trans. Ind. Electron.*, vol. 66, no. 7, pp. 5144-5152, Jul. 2019.

[13] X. Sun, J. Wu, G. Lei, Y. Cai, X. Chen, and Y. Guo, “Torque modeling of a segmented-rotor SRM using maximum-correntropy-criterion-based LSSVR for torque calculation of EVs,” *IEEE J. Emerg. Sel. Topics Power Electron.*, vol. 9, no. 3, pp. 2674-2684, Jun. 2021.

[14] M. A M Cheema, J. E Fletcher, M. Farshadnia, and M. F Rahman, “Sliding mode based combined speed and direct thrust force control of linear permanent magnet synchronous motors with first-order plus integral sliding condition,” *IEEE Trans. Power Electron.*, vol. 34, no. 3, pp. 2526-2538, Mar. 2019.

[15] X. Sun, M. Wu, G. Lei, Y. Guo, and J. Zhu, “An improved model predictive current control for PMSM drives based on current track circle,” *IEEE Trans. Ind. Electron.*, vol. 68, no. 5, pp. 3782-3793, May 2021.

[16] M. Li, J. Zhao, Y. Hu and Z. Wang, "Active disturbance rejection position servo control of PMSLM based on reduced-order extended state observer," *Chinese Journal of Electrical Engineering*, vol. 6, no. 2, pp. 30-41, June 2020.

[17] X. Sun, J. Cao, G. Lei, Y. Guo, and J. Zhu, "A robust deadbeat predictive controller with delay compensation based on composite sliding mode observer for PMSMs," *IEEE Trans. Power Electron.*, vol. 36, no. 9, pp. 10742-10752, Sep. 2021.

[18] S. Song, Z. Xia, G. Fang, R. Ma, and W. Liu, "Phase current reconstruction and control of three-phase switched reluctance machine with modular power converter using single DC-link current sensor," *IEEE Trans. Power Electron.*, vol. 33, no. 10, pp. 8637-8649, Oct. 2018.

[19] Z. Jin, et al, "Sliding mode direct torque control of SPMSMs based on a hybrid wolf optimization algorithm," *IEEE Trans. Ind. Electron.*, 2021. DOI: 10.1109/TIE.2021.3080220, to be published.

[20] H. Wang, X. Ge, and Y. Liu, "Second-order sliding-mode MRAS observer-based sensorless vector control of linear induction motor drives for medium-low speed maglev applications," *IEEE Trans. Ind. Electron.*, vol. 65, no. 12, pp. 9938-9952, Dec. 2018.

[21] X. Sun, J. Wu, G. Lei, Y. Guo, and J. Zhu, "Torque ripple reduction of SRM drive using improved direct torque control with sliding mode controller and observer," *IEEE Trans. Ind. Electron.*, vol. 68, no. 10, pp. 9334-9345, Oct. 2021.

[22] Z. Zhao, H. Gu, J. Zhang, and G. Ding, "Terminal sliding mode control based on super-twisting algorithm," *Journal of Systems Engineering and Electronics*, vol. 28, no. 1, pp. 145-150, 2017.

[23] A. Chalanga, S. Kamal, L. M. Fridman, B. Bandyopadhyay, and J. A. Moreno, "Implementation of super-twisting control: super-twisting and higher order sliding-mode observer-based approaches," *IEEE Trans. Ind. Electron.*, vol. 63, no. 6, pp. 3677-3685, 2016.

[24] H. Du, X. Chen, G. Wen, X. Yu, and Lu. J, "Discrete-time fast terminal sliding mode control for permanent magnet linear motor," *IEEE Trans. Ind. Electron.*, vol. 65, no. 12, pp. 9916-9927, Dec. 2018.

[25] S. Li, M. Zhou, and X. Yu, "Design and implementation of terminal sliding mode control method for PMSM speed regulation system," *IEEE Trans. Ind. Informat.*, vol. 9, no. 4, pp. 1879-1891, Nov. 2013.

[26] J. Qiao, Z. Li, J. Xu, and X. Yu, "Composite nonsingular terminal sliding mode attitude controller for spacecraft with actuator dynamics under matched and mismatched disturbances," *IEEE Trans. Ind. Informat.*, vol. 16, no. 2, pp. 1153-1162, Feb. 2020.

[27] G. Wang, M. Chadli, and B. M, "Practical terminal sliding mode control of nonlinear uncertain active suspension systems with adaptive disturbance observer," *IEEE/ASME Trans. Mechatron.*, pp. 1-1, 2020.

[28] M. J. Neath, A. K. Swain, U. K. Madawala, and D. J. Thrimawithana, "An optimal PID controller for a bidirectional inductive power transfer system using multiobjective genetic algorithm," *IEEE Trans. Power Electron.*, vol. 29, no. 3, pp. 1523-1531, Mar. 2014.

[29] Z. Yang, et al, "Study on active disturbance rejection control of a bearingless induction motor based on an improved particle swarm optimization-genetic algorithm," *IEEE Trans. Transport. Electrific.*, vol. 7, no. 2, pp. 694-705, Jun. 2021.

[30] X. Sun, C. Hu, G. Lei, Y. Guo and J. Zhu, "State Feedback Control for a PM Hub Motor Based on Gray Wolf Optimization Algorithm", *IEEE Trans. Power Electron.*, vol. 35, no. 1, pp. 1136-1146, 2020.

[31] J. Pierezan and L. D. S. Coelho, "Coyote Optimization Algorithm: A New Metaheuristic for Global Optimization Problems", *IEEE CEC, Rio de Janeiro*, Brazil, 2018.

[32] K. Diao, X. Sun, G. Lei, G. Bramerdorfer, Y. Guo, and J. Zhu, "System-level robust design optimization of a switched reluctance motor drive system considering multiple driving cycles," *IEEE Trans. Energy Convers.*, vol. 36, no. 1, pp. 348-357, Mar. 2021.

[33] X. Sun, J. Cao, G. Lei, Y. Guo, and J. Zhu, "A composite sliding mode control for SPMSM drives based on a new hybrid reaching law with disturbance compensation," *IEEE Trans. Transport. Electrific.*, vol. 7, no. 3, pp. 1427-1436, Sep. 2021.

[34] X. Sun, Y. Zhang, G. Lei, Y. Guo, and J. Zhu, "An improved deadbeat predictive stator flux control with reduced-order disturbance observer for in-wheel PMSMs," *IEEE/ASME Trans. Mechatronics*, 2021. DOI: 10.1109/TMECH.2021.3068973, to be published.

[35] S. Chen, N. Cheung, K. Wong and J. Wu, "Integral sliding-mode direct torque control of doubly-fed induction generators under unbalanced grid voltage", *IEEE Trans. Energy Convers.*, pp. 356-368, 2010.

[36] S. Mirjalili, S. Mohammad, and A. Lewis, "Grey wolf optimizer," *Advances in Engineering Software*, vol. 69, no. 3, pp. 46–61, 2014.

[37] M. H. Qais, H. M. Hasanien and S. Alghuwainem, "A grey wolf optimizer for optimum parameters of multiple PI controllers of a grid-connected PMSG driven by variable speed wind turbine", *IEEE Access*, vol. 6, pp. 44120-44128, 2018.

[38] R. Precup, R, David, and E. Petriu, "Grey wolf optimizer algorithm-based tuning of fuzzy control systems with reduced parametric sensitivity," *IEEE Trans. Ind. Electronic.*, vol. 64, no. 1, pp. 527-534, 2017.

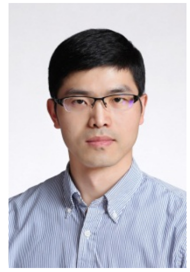

Xiaodong Sun (M'12-SM'18) received the B.Sc. degree in electrical engineering, and the M.Sc. and Ph.D. degrees in control engineering from Jiangsu University, Zhenjiang, China, in 2004, 2008, and 2011, respectively.

Since 2004, he has been with Jiangsu University, where he is currently a Professor in Vehicle Engineering with the Automotive Engineering Research Institute. From 2014 to 2015, he was a Visiting Professor with the School of Electrical, Mechanical, and Mechatronic Systems, University of Technology Sydney, Sydney, Australia. His current teaching and research interests include electrified vehicles, electrical machines, electrical drives, and energy management. He is the author or coauthor of more than 100 refereed technical papers and one book, and he is the holder of 42 patents in his areas of interest. Dr. Sun is an Editor of the IEEE TRANSACTIONS ON ENERGY CONVERSION.

Liyun Feng (S'20) received the B.S. degree in electronic information engineering and M.S. degree in electrical engineering from Jiangsu University, Zhenjiang, China, in 2017 and 2020, respectively. She is currently working toward the Ph.D. degree in Jiangsu University, Zhenjiang, China.

Her research interests include design, analysis and control of high efficiency and energy saving driving switched reluctance motor.

Zhen Zhu received the B.S., M.S., and Ph.D. degrees from the School of Automotive and Traffic Engineering, Jiangsu University, Zhenjiang, China. In 2016, he joined the Automotive Engineering Research Institute, Jiangsu University, as an Assistant Professor. His research interests include artificial intelligence, vehicle dynamics, and control theory.

Gang Lei (M'14) received the B.S. degree in Mathematics from Huanggang Normal University, China, in 2003, the M.S. degree in Mathematics and Ph.D. degree in Electrical Engineering from Huazhong University of Science and Technology, China, in 2006 and 2009, respectively.

He is currently a Senior Lecturer at the School of Electrical and Data Engineering, University of Technology Sydney (UTS), Australia. His research interests include computational electromagnetics, design optimization and control of electrical drive systems and renewable energy systems. He is an Associate Editor of the IEEE TRANSACTIONS ON INDUSTRIAL

ELECTRONICS and an Editor of the IEEE TRANSACTIONS ON ENERGY CONVERSION.

Kaikai Diao (S'18) received the B.S. degree in vehicle engineering from Jiangsu University, Zhenjiang, China, in 2017, and he is currently working toward the Ph.D. degree in Jiangsu University, Zhenjiang, China.

His current research interests include design, optimization, magnetic equivalent circuits modeling, control, and loss analysis of switched reluctance motors for automobile application.

Youguang Guo (S'02-M'05-SM'06) received the B.E. degree from Huazhong University of Science and Technology, China in 1985, the M.E. degree from Zhejiang University, China in 1988, and the Ph.D. degree from University of Technology, Sydney (UTS), Australia in 2004, all in electrical engineering.

He is currently a Professor at the School of Electrical and Data Engineering, University of Technology Sydney (UTS). His research fields include measurement and modeling of properties of magnetic materials, numerical analysis of electromagnetic field, electrical machine design optimization, power electronic drives and control.

Jianguo Zhu (S'93–M'96–SM'03) received the B.E. degree in 1982 from Jiangsu Institute of Technology, Jiangsu, China, the M.E. degree in 1987 from Shanghai University of Technology, Shanghai, China, and the Ph.D. degree in 1995 from the University of Technology Sydney (UTS), Sydney, Australia, all in electrical engineering.

He was appointed a lecturer at UTS in 1994 and promoted to full professor in 2004 and Distinguished Professor of Electrical Engineering in 2017. At UTS, he has held various leadership positions, including the Head of School for School of Electrical, Mechanical and Mechatronic Systems and Director for Centre of Electrical Machines and Power Electronics. In 2018, he joined the University of Sydney, Australia, as a full professor and Head of School for School of Electrical and Information Engineering. His research interests include computational electromagnetics, measurement and modelling of magnetic properties of materials, electrical machines and drives, power electronics, renewable energy systems and smart micro grids.